energies

MDPI

Article

Electrochemical Role of Multifunctional Bismuth-Containing Cuprate Ceramic Additive in ZnO Electrodes for Alkaline Ni-Zn Batteries

Angelina K. Stoyanova-Ivanova [1], Todor E. Vlakhov [1,*], Petar A. Lilov [1], Galia D. Ivanova [2,3], Ognyan S. Dimitrov [2], Antonia E. Stoyanova [2,3] and Yordan G. Marinov [1]

[1] Georgi Nadjakov Institute of Solid State Physics, Bulgarian Academy of Sciences, 72 Tsarigradsko Shosse, 1784 Sofia, Bulgaria; angelina@issp.bas.bg (A.K.S.-I.); peter.lilov@issp.bas.bg (P.A.L.); ymarinov@issp.bas.bg (Y.G.M.)
[2] Institute of Electrochemistry and Energy Systems "Academician Evgeni Budevski", Bulgarian Academy of Sciences, Akad. Georgi Bonchev St, Bl. 10, 1113 Sofia, Bulgaria; galia.ivanova@iees.bas.bg (G.D.I.); ognian.dimitrov@iees.bas.bg (O.S.D.); antonia.stoyanova@iees.bas.bg (A.E.S.)
[3] National Centre of Excellence Mechatronics and Clean Technologies, Bul. Kliment Ohridski 8, 1756 Sofia, Bulgaria
* Correspondence: todor_vlakhov@issp.bas.bg

Abstract

The multifunctional bismuth-containing cuprate ceramic—$Bi_{1.7}Pb_{0.3}Sr_2CaCu_2O_x$ (B(Pb)SCCO 2212)—has been employed as a functional additive at 5 wt.% for the zinc electrode in alkaline Ni-Zn batteries in order to improve electrochemical performance and cycling stability. Our study focuses on the electrochemical role of this additive in a 7 M KOH electrolyte, simulating the battery environment. Cyclic Voltammetry (CV) and Chronopotentiometry (CP) were used to investigate the electrochemical processes occurring during electrode operation. The obtained results reveal that an additional cathodic response associated with the B(Pb)SCCO 2212-containing electrode occurs at potentials preceding the main ZnO/Zn reduction process. The CV curves have shown broad cathodic a broad cathodic response consistent with the electrochemical reduction of Bi- and Cu-containing species originating from the ceramic additive. Since these processes occur before the main ZnO/Zn reduction, the formation of reduced Bi/Cu-containing phases may contribute to charge transport within the active mass and to the reduced polarization observed for the modified electrode. These findings provide a possible electrochemical explanation for the improved behavior of zinc electrodes containing 5 wt.% B(Pb)SCCO 2212.

Keywords: ZnO electrode; multifunctional bismuth-containing cuprate ceramic; electrochemical study; In situ reduction; alkaline electrolyte; nickel-zinc batteries

Check for updates

Academic Editor: Seokgyu Ryu

Received: 6 August 2026
Revised: 4 September 2026
Accepted: 12 September 2026
Published: 15 September 2026

Copyright: © 2026 by the authors. Licensee MDPI, Basel, Switzerland. This article is an open access article distributed under the terms and conditions of the Creative Commons Attribution (CC BY) license.

1. Introduction

As the global transition toward cleaner and more sustainable energy systems accelerates, the development of efficient, safe, and environmentally friendly storage technologies has become a critical priority. Zinc-based batteries, which trace their origins to the eighteenth-century voltaic pile, have evolved into a multi-billion-dollar global industry, with billions of units manufactured annually to power applications ranging from consumer electronics to large-scale industrial systems [1,2].

Rechargeable zinc batteries are particularly compelling due to their unique synergy of safety, affordability, natural material abundance, and robust electrochemical perfor-

mance [2]. In alkaline electrolytes, the zinc electrode exhibits a highly negative reaction potential, affording superior operating voltages and improved energy metrics. Crucially, unlike lithium-ion systems, zinc batteries are inherently nonflammable and far less dependent on scarce critical minerals, rendering them highly attractive for grid-scale storage, residential photovoltaic stabilization, and emerging flexible or wearable electronics [1–4].

Despite this immense potential, the widespread commercialization of Ni/Zn batteries remains severely obstructed by long-standing electrochemical challenges intrinsic to the zinc negative electrode in strongly alkaline media. As comprehensively outlined in recent reviews [3,5], the primary failure modes responsible for capacity fade and poor cycle life include: dendritic growth during charging, which threatens separator integrity; electrode shape change and deformation driven by the high solubility of zincate intermediates; surface passivation via the formation of poorly conductive oxide/hydroxide layers; and continuous corrosion resulting from parasitic hydrogen evolution.

To overcome these kinetic and morphological obstacles, the inclusion of functional additives within the negative electrode's active mass has proven effective [3,5–12]. These additives are typically tailored to singular functions—for example, $Ca(OH)_2$ traps soluble species as insoluble calcium zincate to mitigate shape change [13], while metal oxides such as Bi_2O_3 and PbO suppress hydrogen evolution and undergo electrochemical reduction during charging to form conductive metallic networks [10,14,15]. More recent explorations have extended to silver nanoparticles, conductive polymers, and layered double hydroxides (LDHs) [6,7,16,17].

Among these, a highly promising class of additives is conductive bismuth-containing cuprate ceramics with a composition $Bi_{1.7}Pb_{0.3}Sr_2CaCu_2O_x$ (B(Pb)SCCO) 2212 [8], belonging to the Bi–Sr–Ca–Cu–O (BSCCO) system. With the chemical formula $Bi_2Sr_2Ca_{n1}Cu_nO_{2n+4+x}$, bismuth strontium calcium copper oxide (BSCCO) is frequently a multi-phase ceramic cuprate superconductor, with lead typically replacing some of the bismuth [18]. Phases Bi-2201 (T_C = 8 K), Bi-2212 (T_C = 85 K), and Bi-2223 (T_C = 110 K) are frequently mentioned [19]. The first high-temperature superconductor without a rare-earth element with a critical temperature higher than nitrogen's boiling point was the BSCCO superconductor, which was found in 1988 [20]. Among the most researched cuprate superconductors, BSCCO has been used in power technologies, magnets, fault current limiters, and magnetic field shields.

The cuprate ceramic with a composition $Bi_{1.7}Pb_{0.3}Sr_2CaCu_2O_x$ (B(Pb)SCCO) 2212, however, stands out due to its multifunctionality when used as an additive to a zinc electrode. During charging, the ceramic undergoes electrochemical reduction, yielding reduction products that form a percolative, highly conductive metallic network—thereby drastically lowering overall battery resistance. Furthermore, our previous studies have demonstrated that B(Pb)SCCO 2212 mitigates electrode shape change, effectively improving morphological stability [8]. Thus, this single additive concurrently addresses three major failure modes—poor conductivity, corrosion, and structural deformation—offering a distinct advantage over conventional single-function agents [21–23]. It is important to note that its beneficial action is not rooted in its own intrinsic conductivity or superconducting properties.

The introduction of this multifunctional additive has been optimized, establishing that a concentration of 5 wt.% yields superior electrical performance, with notably lower losses compared to 7 wt.% and 10 wt.%, an effect attributed to improved surface properties of the electrode layer [22,23]. While these studies conclusively confirmed the structural and macroscopic electrical advantages of B(Pb)SCCO 2212 addition at 5 wt.%, the precise electrochemical mechanism of the additive has remained undetermined.

More specifically, the contribution of its constituent elements—bismuth (Bi) and copper (Cu)—to the electrochemical behaviour of the zinc electrode has not yet been clarified. To

address this knowledge gap, this study systematically investigated zinc electrodes modified with 5 wt% B(Pb)SCCO 2212, using cyclic voltammetry (CV) and chronopotentiometry. The electrochemical results revealed an additional reduction process preceding the main ZnO/Zn reduction, which provides new insights into the electrochemical transformations associated with the additive. Furthermore, the observed electrochemical processes were correlated with electrode morphology and battery performance to elucidate the relationship between the additive-induced changes in electrode structure, electrochemical behaviour and overall electrode performance.

2. Materials and Methods

2.1. Materials

To investigate the volt-ampere characteristics with a multifunctional bismuth-containing cuprate ceramic (5 wt.% B(Pb)SCCO 2212), the ZnO electrodes described below were synthesized using the technology/ methodology described in [23].

Ceramics of the nominal composition $Bi_{1.7}Pb_{0.3}Sr_2CaCu_2O_x$ (B(Pb)SCCO 2212) were synthesized using the solid-state reaction method. High-purity bismuth oxide (Bi_2O_3), lead oxide (PbO), strontium carbonate ($SrCO_3$), calcium carbonate ($CaCO_3$), and copper oxide (CuO) (99.9%) served as starting materials for solid-phase synthesis. These precursors were individually dried and weighed according to their stoichiometric ratios. Following initial mixing, grinding, and heat treatment at 780 °C for 24 h in air, the resulting powder was re-ground and pressed into a pellet at 5–6 MPa. Subsequent sintering of the B(Pb)SCCO 2212 occurred in air at 830 °C for 48 h. This pellet was homogenized for 90 min, after which samples were taken for X-ray analysis and for use as an additive.

Two types of working electrodes were prepared: a composite electrode containing a ceramic additive, and a comparison electrode without a ceramic additive. The composite electrodes were fabricated using powdered ZnO (NZnO50, Anhui Elite Industrial Co., Ltd., Hong Kong Elite Industrial Group Limited, Hefei, China) as the active material, with 5 wt.% powdered B(Pb)SCCO as the additive, 12% acetylene black, 2 wt.% polytetrafluoroethylene (PTFE) and 1 wt.% carboxymethyl cellulose (CMC) as binding agents. The paste was uniformly deposited onto the pre-fabricated nickel foam (15 mm diameter). The reference electrodes were prepared using the same procedure, but without adding B(Pb)SCCO. The active mass was homogenised by ultrasonic treatment at room temperature (23 °C) using a laboratory sonicator (Hangzhou Dowell Ultrasonic Tech Co., Ltd., Hangzhou, China) operating at 20 kHz and with a power output of 1200 W [23].

Our previous findings indicated that mechanical blending of the active components led to an inhomogeneous electrode mass, a deficiency particularly pronounced concerning the ceramic additive. Therefore, to enhance homogeneity, ultrasonic mixing is adopted for the preparation of the electrode material in this publication. The electrode mass obtained was mixed with distilled water to form a paste, which was then evenly applied to a nickel foam matrix, dried at 70 °C, and pressed at 30 MPa. The dimensions of the pasted Zn electrode layered deposits were 2.0 × 2.0 cm (thickness 1.5 mm) [23].

The electrolyte used in the measurements was 7 M KOH. Water solutions of KOH around 32% (w/w) are commonly used to minimize losses due to electrolyte resistance since concentration values above or below this range reduce electrolyte conductivity [24,25].

2.2. Experimental Methods

For the comprehensive structural and morphological characterization of the synthesized ceramic samples and the prepared zinc active mass incorporating a ceramic additive, standard X-ray diffraction (XRD) and scanning electron microscopy (SEM) were employed.

X-ray diffraction analysis was conducted using a Philips PW 1030 X-ray diffractometer (Philips, Singapore) configured with θ-2θ Bragg–Brentano geometry; Cu Kα radiation lambda = 1.5406 Å, generated at 30 kV and 20 mA, was utilized. Diffraction patterns were acquired at room temperature with a constant scanning speed, covering a 2θ range from 5° to 90° with a step size of 0.04°, and detected by a scintillation detector. Interpretation of the obtained diffraction patterns was performed using the PCPDFWIN database (ICDD, 2002).

The surface morphology of the samples was studied with scanning electron microscopy (SEM) using a Zeiss Evo 10 microscope (Carl Zeiss Microscopy, Oberkochen, Germany). The images were taken in secondary electron mode at an accelerating voltage of 25 keV, with no conductive coating on the samples.

The chemical composition of the surface was studied using electron dispersive spectroscopy (EDS) probe Oxford Ultim Max 40 (Oxford Instruments, Abingdon, UK). The results were compiled with AZtec software (version 6.1 HF4).

All electrochemical characterizations were performed using a Bio-logic SP-200 potentiostat (Bio-Logic Science Instruments, Seyssinet-Pariset, Grenoble, France)/galvanostat in a 7 M KOH electrolyte at a temperature of 25 °C, with potential referenced to a saturated calomel electrode (SCE) and a polished platinum plate as the counter-electrode (CE).

Chronopotentiometry (CP) was conducted at a constant cathodic current of 2 mA for 30 min. Cyclic voltammetry (CV) was carried out using the same cell configuration for three scans within the potential window of −1.2 V to +1.8 V vs. SCE, starting from the open-circuit potential in the positive direction at a rate of 5 mVs^{-1}.

Electrochemical charge/discharge tests were conducted utilizing an automated test system (PMC10), capable of systematically controlling and monitoring experimental parameters during cyclic operation. The tests followed a pre-defined algorithm, which included the following sequential steps:

Charging (Constant Current): A constant current of 0.05 A was applied until the cell potential reached 1.9 V.

Charging (Constant Voltage): Constant voltage charging at 1.9 V ensued, either until the current tapered to $\leq$0.02 A or a maximum duration of 10 h was attained.

Discharging (Constant Current): Discharge was performed at a constant current of 0.05 A, terminating when the cell potential decreased to 1.3 V.

3. Result and Discussion

3.1. X-Ray Diffraction (Xrd)

The X-ray diffraction (XRD) pattern of the B(Pb)SCCO 2212 conductive ceramic is presented in Figure 1.

The diffractogram confirms the presence of the characteristic peaks of the conductive ceramic BSCCO, which are consistent with the crystallographic data for $Bi_2Sr_2CaCu_2O_8$ (PDF card: 00-080-0396). There are no visible secondary phases present. This indicates the high phase purity of the synthesised ceramic.

The main diffraction peak, indexed as (105) for the tetragonal Bi-2212 structure, is observed at 27.48° (2θ). This is compared to 27.41° for the reference Bi-2212 structure. According to Bragg's law, this shift towards higher diffraction angles corresponds to a slight decrease in the interplanar spacing. While such a deviation from the reference position may be associated with structural modifications resulting from Pb incorporation, the available XRD data do not permit this effect to be attributed exclusively to Pb substitution.

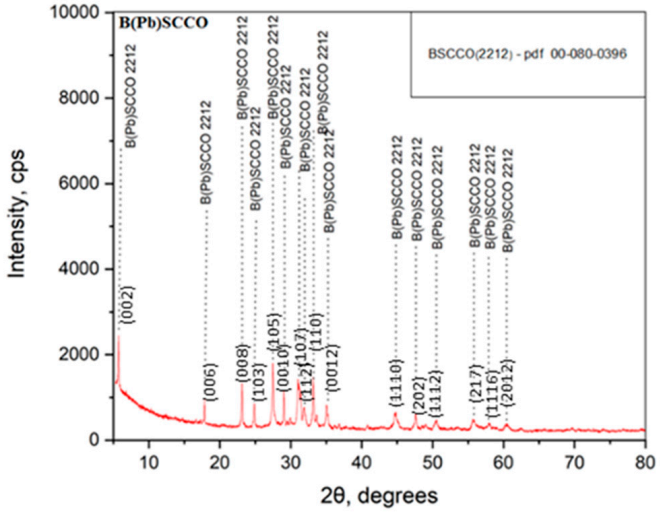

Figure 1. X-ray diffraction pattern of B(Pb)SCCO 2212.

Further XRD analysis was performed on the zinc active mass containing the ceramic additive, as shown in Figure 2**.** The obtained XRD pattern confirms the preservation of the main phase (zinc active mass) and the occurrence of the composite electrode material components, as evidenced by the characteristic reflections of Teflon, graphitised acetylene black and the Bi-2212 ceramic additive. The presence of BSCCO is indicated by the corresponding diffraction peaks, which are relatively weak due to the predominance of zinc active mass. For greater clarity, an expanded intensity scale is used in Figure 2b to highlight the weak BSCCO-related reflections. These results confirm the presence of the Bi-2212 ceramic additive in the composite electrode material.

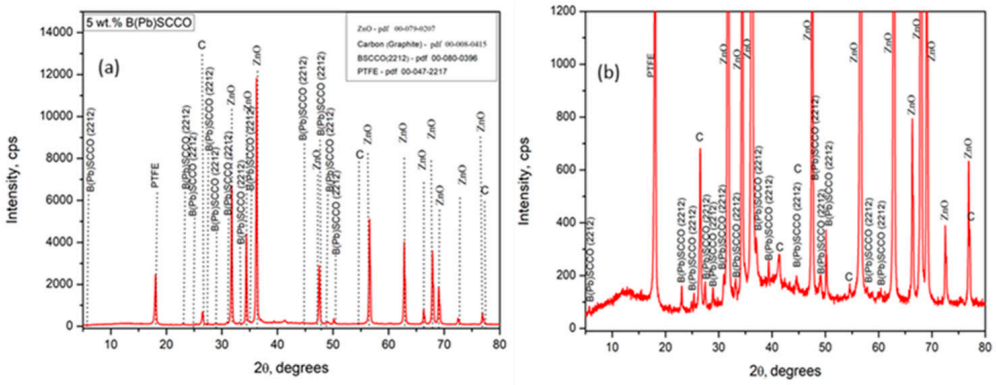

Figure 2. X-ray diffraction pattern of ZnO active mass with an additive of 5 wt.% B(Pb)SCCO 2212. (**a**) ZnO active mass with an additive of 5 wt.% B(Pb)SCCO 2212; (**b**) intensity scale of zinc active mass with an additive of 5 wt.% B(Pb)SCCO 2212.

The crystallite size (D) was estimated from the broadening of the selected diffraction peaks using the Scherrer equation: $D = 0.9\lambda/(\beta \cos \theta)$, where λ is the X-ray wavelength (1.5406 Å), β is the full width at half maximum (FWHM) of the diffraction peak, expressed in radians and θ is the corresponding Bragg angle.

Table 1 presents the calculated crystallite sizes from the three most intense and well-resolved reflections of each crystalline phase. It also provides the corresponding references used for the calculation of the D-values, as reported in [26]. The instrumental contribution to peak broadening was determined using a standard reference material, and the corrected full width at half maximum (FWHM) values were used in the calculations.

Table 1. Crystallite size of the conductive ceramic and composite electrode.

Sample		(hkl)	2θ	θ	cos θ	β_{corr} (rad)	D [nm]
Conductive ceramic B(Pb)SCCO 2212		(105)	27.46	13.73	0.9714	0.002485	57.43
		(110)	33.16	16.58	0.9584	0.003057	47.33
		(107)	30.94	15.495	0.9637	0.002899	49.63
Composite electrode	5 wt.% B(Pb)SCCO 2212 (ceram. additive)	(105)	27.43	13.72	0.9715	0.003549	40.22
		(110)	33.16	16.58	0.9584	0.004479	32.30
		(107)	30.97	15.485	0.9637	0.008428	17.07
	ZnO (active mass)	(101)	36.18	18.09	0.9504	0.002907	50.18
		(100)	31.69	15.875	0.9619	0.002719	53.02
		(002)	34.396	17.198	0.9553	0.002671	54.33

The average crystallite size of the conductive ceramic was approximately 51 nm. When the ceramic was present as an additive in the zinc active mass, the diffraction peaks were weaker and affected by the contribution of the surrounding matrix, resulting in a lower calculated average crystallite size of approximately 30 nm. For ZnO, the calculated values were relatively consistent, with an average crystallite size of approximately 53 nm.

3.2. Scanning Electron Microscopy (Sem) and Energy Dispersive Spectroscopy (EDS)

The surface morphology of the electrode active mass is a critical parameter influencing its operational characteristics. Figure 3a,b presents SEM images of the pure zinc electrode and zinc active mass supplemented with 5 wt.% B(Pb)SCCO 2212. The images at lower magnification (3000 times) clearly illustrate a homogeneous distribution of both ceramic particles and carbon throughout the active mass, while the ones at higher magnification (30,000 times) reveal fine crystals with dimensions between 50–300 nm.

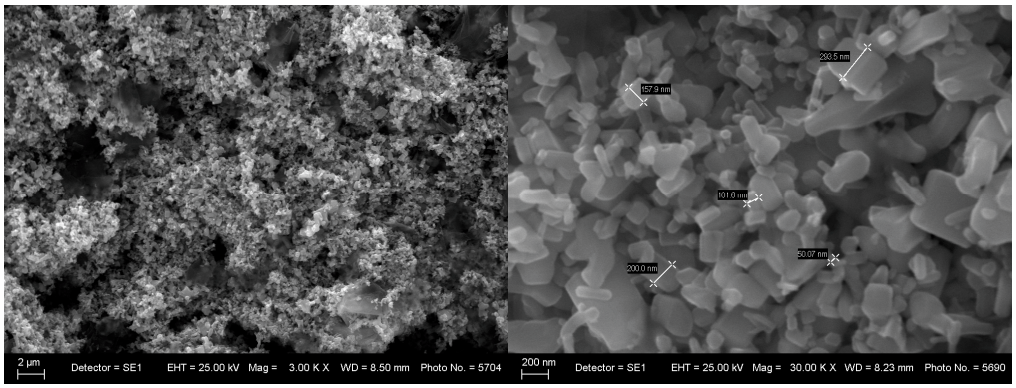

(**a**)

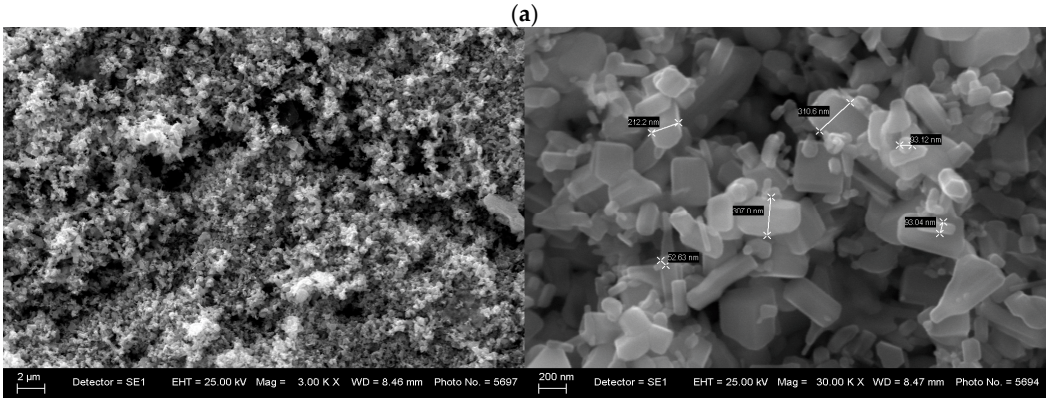

(**b**)

Figure 3. *Cont.*

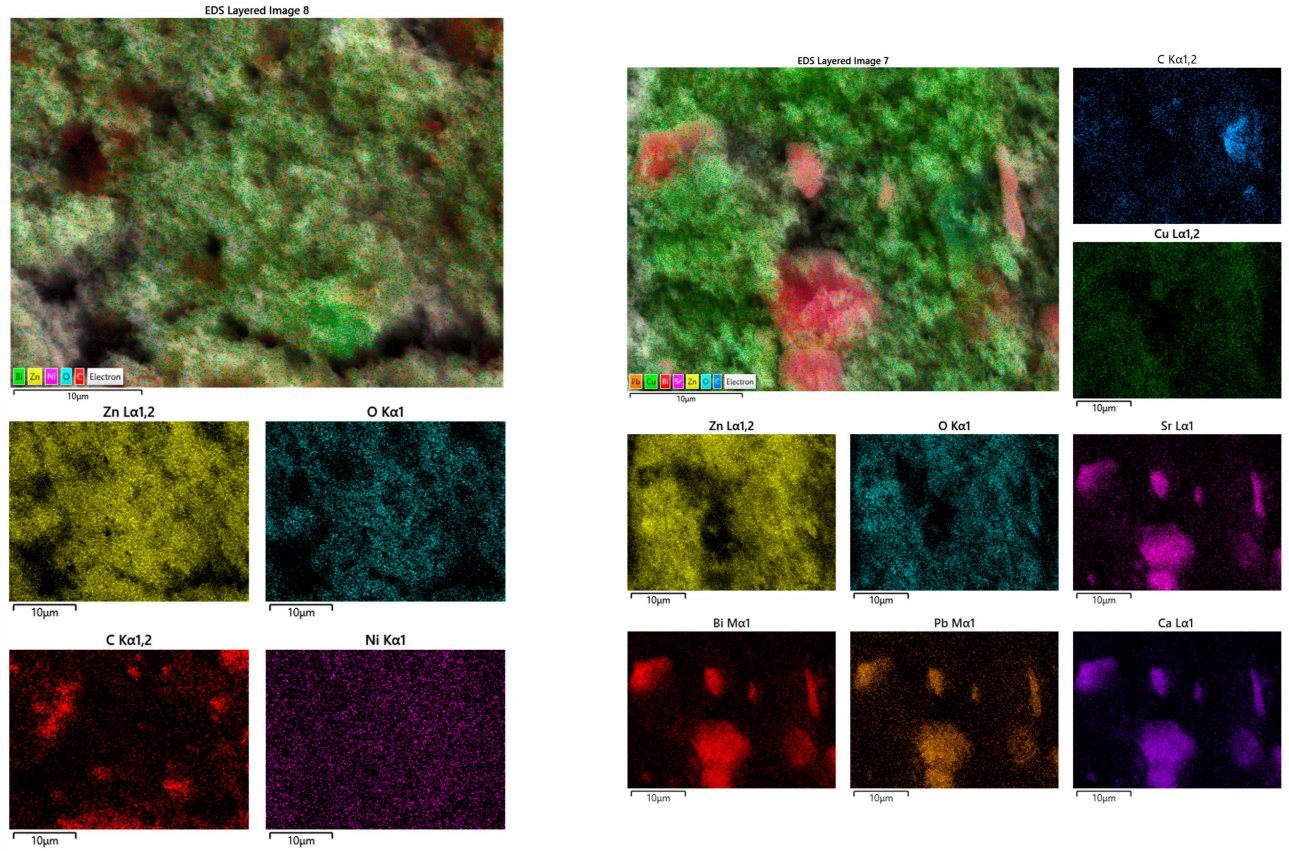

(**c**) (**d**)

Figure 3. (**a**) SEM images of ZnO active mass without additive with magnifications of 3000 (left) and 30,000 times (right). (**b**) SEM images of ZnO active mass with 5 wt.% B(Pb)SCCO 2212 with magnifications of 3000 (left) and 30,000 times (right). (**c**) EDS analysis of ZnO electrode mass. (**d**) EDS analysis of ZnO electrode mass with an additive of 5 wt.%B(Pb)SCCO 2212.

The chemical composition of the active mass was studied with energy-dispersive spectroscopy (EDS) and the corresponding elemental maps are presented in Figure 3c,d. The analysis revealed that both electrodes show strong peaks at 1.01 keV and 0.53 keV which correspond to the characteristic Lα and Kα lines of Zn and O respectively. Lower-intensity signals associated with Cu, Sr, Pb, Bi and Ca can be registered in the sample with additive. The average elemental composition is calculated from the EDS spectra and is presented in Table 2 as atomic percentage. It is evident that no significant compositional changes occurred after ultrasonic mixing, ensuring the integrity of the active components.

Table 2. EDS analysis of ZnO electrode mass without and with an additive of 5 wt.% B(Pb)SCCO 2212.

Element (at%)	C	O	Ni	Cu	Zn	Sr	Pb	Bi	Ca	Total
Electrode without additive	69.5	17.65	0.36	-	12.5	-	-	-	-	100
Electrode with additive	33.61	33.4	0.15	0.55	29.88	0.62	0.12	1.16	0.51	100

3.3. Chronopotentiometry (Cp)

The initial electrochemical reduction behavior of the pure and doped ZnO electrodes was investigated using chronopotentiometry, as shown in Figure 4.

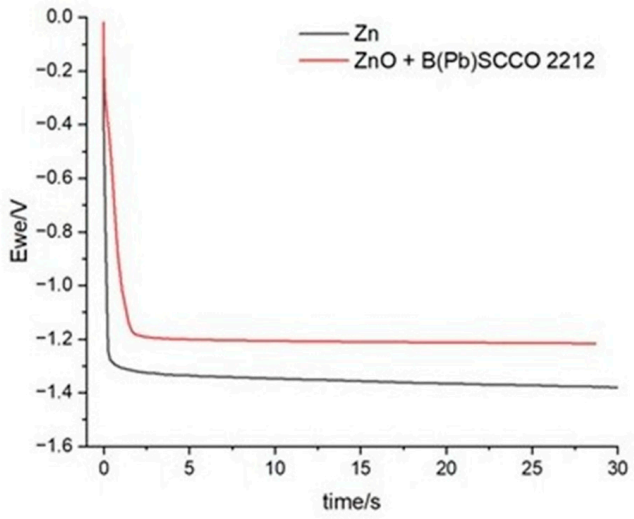

Figure 4. Potential vs. time curves of the chronopotentiometry experiment for ZnO and ZnO with 5 wt.% B(Pb)SCCO 2212.

The unmodified ZnO electrode stabilized at a potential plateau of approximately −1.4 V (vs. SCE). In contrast, the electrode containing the B(Pb)SCCO additive operated at a significantly less negative potential of approximately −1.2 V (vs. SCE).

The unmodified ZnO electrode stabilised at a potential plateau of approximately −1.4 V (relative to SCE). By contrast, the electrode containing the B(Pb)SCCO additive operated at a less negative potential of around −1.2 V (relative to SCE). The resulting potential difference of around 200 mV suggests reduced polarization under the applied current conditions. This shift is consistent with the altered electrochemical response of the composite electrode.

This behaviour suggests that the B(Pb)SCCO 2212 additive affects the electrochemical kinetics of the zinc electrode.

The electrochemical activity of the Bi- and Cu-containing components may contribute to the observed change in polarization and charge-transfer behavior.

This improved reaction is consistent with the morphological observations presented in Figure 3, which show that the presence of B(Pb)SCCO 2212 leads to a more homogeneous electrode structure. A more uniform distribution of active components may contribute to a more uniform current distribution, reducing localised electrochemical activity. These factors are important for improving the stability of the zinc electrode.

The observed reduction in polarization is also consistent with previously published electrochemical impedance spectroscopy (EIS) results, which demonstrated reduced charge transfer resistance for B(Pb)SCCO 2212-containing electrodes compared to unmodified zinc electrodes [22,23]. These findings support the role of the ceramic additive in enhancing the charge transfer characteristics of the zinc electrode.

3.4. Cyclic Voltammetry (Cv)

Further information regarding the electrochemical behaviour of the electrodes was obtained by means of cyclic voltammetry (see Figures 5–7).

The cyclic voltammogram of the unmodified ZnO electrode (Figure 5) does not show a clearly distinguishable redox peak within the potential range studied. At higher positive potentials, a marked increase in the anodic current is observed, which is primarily attributed to the oxygen evolution reaction.

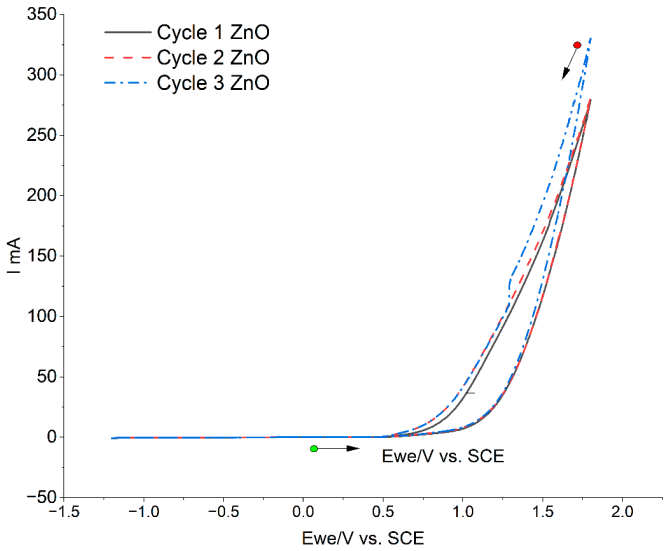

Figure 5. CV curves (first, second, and third cycles) of the unmodified ZnO electrode in 7 M KOH solution at a scan rate of 5 mV s^{-1}. The green arrow indicates oxidation. The red arrow indicates reduction.

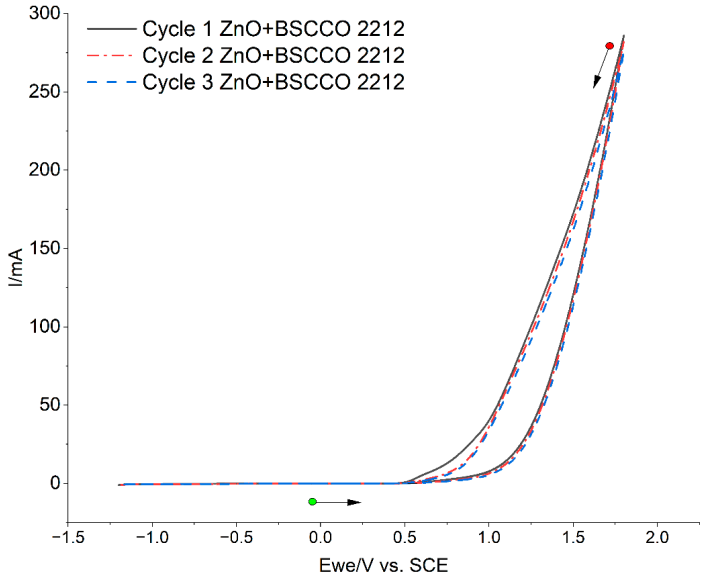

Figure 6. CV curves (first, second, and third cycles) of the ZnO electrode modified with 5 wt.% B(Pb)SCCO 2212 in 7 M KOH solution at a scan rate of 5 mV s^{-1}. The green arrow follows oxidation. The red arrow is reduction.

The ZnO electrode modified with B(Pb)SCCO 2212 (Figure 6) exhibits an altered voltammetric response compared with the unmodified ZnO electrode. It is evident that differences in the current response become apparent in the medium-to-high positive potential region. However, the present CV curves do not clearly show any distinguishable cathodic peak. Consequently, the observed response is characterised as an additional electrochemically active contribution of the B(Pb)SCCO 2212-containing electrode, rather than being unequivocally ascribed to a particular reduction process involving Bi or Cu.

This reaction is absent in the unmodified electrode and corresponds to the electrochemical reduction of Bi- and Cu-containing compounds originating from the ceramic additive.

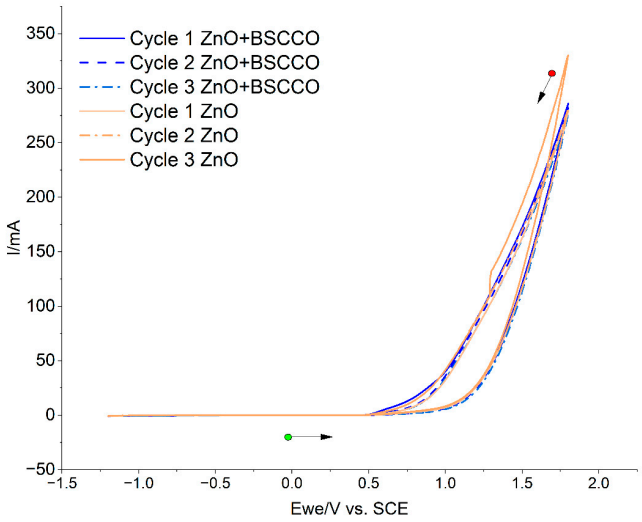

Figure 7. Comparison of the first, second, and third CV cycles of unmodified ZnO and ZnO modified with 5 wt.% B(Pb)SCCO 2212 in 7 M KOH solution at a scan rate of 5 mV s^{-1}. The green arrow follows oxidation. The red arrow is reduction.

This behaviour differs from that observed in pure B(Pb)SCCO-type ceramics, as described earlier [8], where distinct reduction peaks were identified. This difference is due to a different electrode configuration. In the previous study, the ceramic was investigated as an electrochemically active material; in the present study, however, it acts only as 5 wt.% additive dispersed in the active ZnO matrix.

As demonstrated in Figure 7, the incorporation of 5 wt.% B(Pb)SCCO 2212 modifies the overall voltammetric behaviour of the ZnO electrode. The difference between the two electrodes is particularly evident in the anodic current region, where the B(Pb)SCCO 2212-containing electrode exhibits a modified current response compared with unmodified ZnO. At higher positive potentials, both electrodes show a pronounced increase in anodic current, which is consistent with the oxygen evolution reaction.

The individual redox processes associated with Bi and Cu cannot be resolved as distinct peaks in the present CV measurements. The differences in the voltammetric responses of the B(Pb)SCCO 2212-containing and unmodified ZnO electrodes indicate that the ceramic additive influences the overall electrochemical behaviour of the ZnO-based electrode.

It is important to note that the reduction processes associated with the B(Pb)SCCO 2212 additive occur at more positive potentials than the main ZnO/Zn reduction process under the respective experimental conditions. This suggests that Bi- and Cu-containing compounds participate in electrochemical reduction before the main ZnO/Zn reduction step. The resulting reduced phases may contribute to charge transport in the active mass. However, it is not possible to determine their final oxidation states unambiguously based on the present characterisation.

The early formation of these conductive phases, together with the improved microstructure observed using SEM, provides a plausible explanation for the modified electrode's improved electrochemical characteristics. The conductive Bi/Cu regions facilitate electron transport within the active mass, resulting in lower polarization and faster charge transfer, which is consistent with chronopotentiometric measurements. This interpretation is further supported by EIS results showing a significant reduction in charge transfer resistance (Rct) for the modified electrode [22,23]. The more homogeneous current distribution may also suppress localised zinc deposition, thereby reducing dendrite formation and surface passivation.

3.5. Electrochemical Charge/Discharge Tests

The charge/discharge profiles of the zinc electrode containing the B(Pb)SCCO 2212 additive are presented in Figure 8. The cell was charged using a constant-current/constant-voltage (CC–CV) protocol, with a constant current of 0.05 A applied until the cell voltage reached 1.9 V, followed by constant-voltage charging at 1.9 V until the current decreased to $\leq$0.02 A or a maximum charging time of 10 h was reached. Discharge was subsequently performed at a constant current of 0.05 A until the cell voltage decreased to 1.3 V. The electrode exhibited stable charge/discharge behavior over consecutive cycles, with a coulombic efficiency of 85–90%, indicating good reversibility of the ZnO/Zn electrochemical reactions.

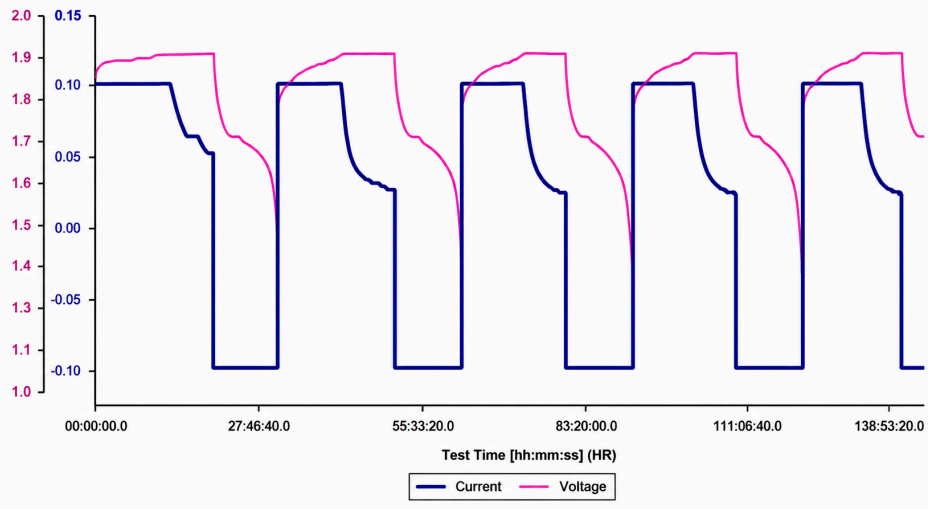

Figure 8. Voltage and current profiles of the zinc electrode containing 5 wt.% B(Pb)SCCO 2212 additive during long-term cycling.

This improved electrochemical reaction may be due to the combined effect of several factors. The B(Pb)SCCO 2212 additive introduces electrochemically active Bi- and Cu-containing compounds, which are reduced at potentials preceding the main ZnO reduction process. Furthermore, SEM analysis revealed that the presence of the ceramic additive contributes to improved electrode morphology, leading to a more homogeneous distribution of the active components.

These characteristics can facilitate charge transfer and promote a more uniform electrochemical reaction throughout the electrode's entire volume, which is an important factor in improving the stability of zinc electrodes in alkaline Ni–Zn battery systems.

4. Conclusions

This study demonstrates that the incorporation of 5 wt.% of the conductive ceramic B(Pb)SCCO 2212 into the active mass of zinc electrodes has a positive influence on the electrochemical behaviour of Ni–Zn battery electrodes.

Structural and morphological investigations confirmed the successful incorporation of the ceramic additive into the ZnO-based electrode matrix. XRD analysis revealed no undesired crystalline phase formation during electrode preparation, while SEM and EDS analyses showed a more homogeneous distribution of the additive components within the active mass.

Electrochemical studies conducted using chronopotentiometry and cyclic voltammetry provided insight into the role of B(Pb)SCCO 2212 during electrode operation. The additive introduces electrochemically active compounds containing bismuth (Bi) and copper (Cu), which are reduced at more positive potentials than those of the main ZnO/Zn reduction process. While this characterisation does not determine the precise oxidation states of these

compounds, the results are consistent with electrochemical reduction and the formation of reduced phases containing Bi and Cu.

The presence of these regions, together with the improved morphological uniformity of the composite electrode, improves charge transport characteristics and reduces electrode polarization. This improved electrochemical performance is consistent with previously published impedance measurements showing reduced charge transfer resistance for electrodes modified with B(Pb)SCCO 2212.

The combined structural and electrochemical effects suggest that B(Pb)SCCO 2212 acts as a multifunctional additive, providing the following:

- Electronic contribution: improvement of charge transport pathways through the formation of electrochemically generated conductive phases containing Bi and Cu;
- Structural contribution: modification of electrode morphology and potential stabilisation of zinc deposition processes.

Overall, the results demonstrate the potential of conductive cuprate ceramics as additives to improve the electrochemical performance and stability of zinc electrodes in alkaline Ni–Zn battery systems.

Author Contributions: Conceptualization, A.K.S.-I. and Y.G.M.; Methodology, A.K.S.-I., A.E.S. and Y.G.M.; Formal analysis, T.E.V., P.A.L., G.D.I. and O.S.D.; Investigation, A.K.S.-I., T.E.V., P.A.L., G.D.I. and O.S.D.; Writing—original draft, A.K.S.-I., T.E.V. and P.A.L.; Writing—review & editing, A.K.S.-I. and A.E.S. All authors have read and agreed to the published version of the manuscript.

Funding: This research was funded by the "National Center of Excellence 'Mechatronics and Clean Technologies'" (BG16RFPR002-1.014-0006) under the "Research, Innovation and Digitalization for Smart Transformation" Programme 2021–2027.

Data Availability Statement: The original contributions presented in the study are included in the article, further inquiries can be directed to the corresponding author.

Acknowledgments: The authors would like to express their sincere gratitude to Mariela Dimitrova for conducting the X-ray diffraction analyses and for her valuable contribution to the characterization of the investigated materials.

Conflicts of Interest: The authors declare no conflict of interest.

References

1. Bello, I.T.; Raza, H.; Michael, A.T. Charging Ahead: The Evolution and Reliability of Nickel-Zinc Battery Solutions. *EcoMat* **2025**, *7*, e12505. [CrossRef]
2. Clark, S. Batteries–Battery Types–Zinc Batteries Overview. In *Encyclopedia of Electrochemical Power Sources*, 2nd ed.; Elsevier: Amsterdam, The Netherlands, 2025; Volume 3, pp. 747–759. [CrossRef]
3. Wang, N.; Li, M.; Cao, M.; Yin, Y. Research progress of zinc-nickel battery anode materials: Challenges and development strategies. *Ionics* **2025**, *31*, 1181–1201. [CrossRef]
4. Liu, X.; Wang, H.; Fan, X. Stabilizing zinc anodes for long-lifespan zinc–nickel battery through the in-situ construction of zincophilic interface layer. *Energy Storage Mater.* **2023**, *58*, 311–321. [CrossRef]
5. Gong, Y.; Wang, B.; Ren, H. Recent Advances in Structural Optimization and Surface Modification on Current Collectors for High-Performance Zinc Anode: Principles, Strategies, and Challenges. *Nano-Micro Lett.* **2023**, *15*, 208. [CrossRef] [PubMed]
6. Rong, Y.; Yang, Z.; Deng, L.; Fu, Z. ZnO@Ag microspheres used as the anodic materials of superior alkaline rechargeable Zn–Ni batteries. *Ceram. Int.* **2020**, *46*, 16908–16917. [CrossRef]
7. Yang, B.; Yang, Z.; Peng, Z.; Liao, Q. Effect of silver additive on the electrochemical performance of ZnAl-layered double hydroxide as anode material for nickel-zinc rechargeable batteries. *Electrochim. Acta* **2014**, *132*, 83–90. [CrossRef]
8. Stoyanova-Ivanova, A.; Lilov, P.; Vasev, A. Studies of structural and morphological properties of cuprate conductive ceramics after electrochemical treatment in alkaline electrolyte. *Mater. Chem. Phys.* **2020**, *239*, 121934. [CrossRef]
9. Huang, H.; Zhang, L.; Zhang, W.K.; Gan, Y.P.; Shao, H. Preparation and electrochemical properties of ZnO/conductive-ceramic nanocomposite as anode material for Ni/Zn rechargeable battery. *J. Power Sources* **2008**, *184*, 663–667. [CrossRef]

10. Cheng, J.; Zhang, Z.; Zhao, Y.; Yu, W.; Hou, H. Effects of additives on performance of zinc electrode. *Trans. Nonferrous Met. Soc. China* **2014**, *24*, 3551–3555. [CrossRef]
11. Jindra, J. Progress in sealed Ni-Zn cells, 1991–1995. *J. Power Sources* **1997**, *66*, 15–25. [CrossRef]
12. Shukla, A.K.; Venugopalan, S.; Hariprakash, B. Nickel-based rechargeable batteries. *J. Power Sources* **2001**, *100*, 125–148. [CrossRef]
13. Tan, Z.; Yang, Z.; Ni, X.; Chen, H.; Wen, R. Effects of calcium lignosulfonate on the performance of zinc–nickel battery. *Electrochim. Acta* **2012**, *85*, 554–559. [CrossRef]
14. Caldeira, V.; Rouget, R.; Fourgeot, F. Controlling the shape change and dendritic growth in Zn negative electrodes for application in Zn/Ni batteries. *J. Power Sources* **2017**, *350*, 109–116. [CrossRef]
15. Shivkumar, R.; Kalaignan, G.P.; Vasudevan, T. Studies with porous zinc electrodes with additives for secondary alkaline batteries. *J. Power Sources* **1998**, *75*, 90–100. [CrossRef]
16. San José, M.T.; Espinosa, A.M.; Tascón, M.L.; Vásquez, M.D.; Sánchez Batanero, P. Electrochemical behaviour of copper oxides at a carbon paste electrode. Application to the study of the superconductor YBaCuO. *Electrochim. Acta* **1991**, *36*, 1209–1218. [CrossRef]
17. Fan, X.; Yang, Z.; Wen, R.; Yang, B.; Long, W. The application of Zn–Al-hydrotalcite as a novel anodic material for Ni–Zn secondary cells. *J. Power Sources* **2013**, *224*, 80–85. [CrossRef]
18. Hudakova, N.; Plechacek, V.; Dordor, P.; Flachbart, K.; Knizek, K.; Kovac, J.; Reiffers, M. Influence of PB concentration on microstructural and superconducting properties of BSCCO superconductors. *Supercond. Sci. Technol.* **1995**, *8*, 324. [CrossRef]
19. Lim, C.S.; Wang, L.; Chua, C.K.; Sofer, Z.; Jankovský, O.; Pumera, M. High temperature superconducting materials as bi-functional catalysts for hydrogen evolution and oxygen reduction. *J. Mater. Chem. A* **2015**, *3*, 8346–8352. [CrossRef]
20. Maeda, H.; Tanaka, Y.; Fukutomi, M.; Asano, T. A new high-Tc oxide superconductor without a rare-earth element. *Jpn. J. Appl. Phys.* **1988**, *27*, 209. [CrossRef]
21. Mladenov, M.; Raicheff, R.; Stoyanov, L.; Stoyanova-Ivanova, A.; Terzieva, S.; Kovacheva, D. Electrode Mass for Zinc Electrode of Alkaline Rechargeable Batteries. BG Patent Reg. No 66730/28.8.2018, 28 August 2018. (In Bulgarian)
22. Stoyanova-Ivanova, A.K.; Lefterova, E.D.; Ivanova, G.D.; Marinov, Y.G.; Hadjichristov, G.B.; Stoyanova, A.E. Impedance spectroscopy study of Ni-Zn electrochemical alkaline systems with anode of nano-sized ZnO doped with conducting ceramics B(Pb)SCCO 2212. *Comptes Rendus l'Académie Bulg. Sci.* **2022**, *75*, 358–366. [CrossRef]
23. Stoyanova-Ivanova, A.K.; Lefterova, E.D.; Marinov, Y.G.; Ivanova, G.D.; Stoyanova, A.E.; Hadjichristov, G.B. Electrochemical cells with anodes performed with Zn active mass with added B(Pb)SCCO 2212 conductive ceramics. *Comptes Rendus l'Académie Bulg. Sci.* **2023**, *76*, 871–878. [CrossRef]
24. Gilliam, R.J.; Graydon, J.W.; Kirk, D.W.; Thorpe, S.J. A review of specific conductivities of potassium hydroxide solutions for various concentrations and temperatures. *Int. J. Hydrogen Energy* **2007**, *32*, 359–364. [CrossRef]
25. Sánchez, M.; Amores, E.; Rodríguez, L.; Clemente-Jul, C. Semi-empirical model and experimental validation for the performance evaluation of a 15 kW alkaline water electrolyzer. *Int. J. Hydrogen Energy* **2018**, *43*, 20332–20345. [CrossRef]
26. Zaman, M.; Alotaibi, B.M.; Jawhari, A.H.; Alyousef, H.A.; Alrowaily, A.W.; Faizan, M.; Ahmad, N. Fabrication and electrochemical investigation of MnCo2O4/PANI nanohybrid for supercapacitor. *J. Sol-Gel Sci. Technol.* **2025**, *116*, 1464–1476. [CrossRef]

Disclaimer/Publisher's Note: The statements, opinions and data contained in all publications are solely those of the individual author(s) and contributor(s) and not of MDPI and/or the editor(s). MDPI and/or the editor(s) disclaim responsibility for any injury to people or property resulting from any ideas, methods, instructions or products referred to in the content.